The molecular role of Serf2 in development and misfolded protein aggregation

Stroo, Esther

Chapter 3

Full-body deletion of *Serf2* causes growth retardation, fetal atelectasis and neonatal death in mice

Esther Stroo[1], Leen Janssen[1], Olga Sin[1], Wytse Hogewerf[1], Bjorn Bakker[1], Mirjam Koster[2], Liesbeth Harkema[3], Sameh Youseef[2,3], Bart van de Sluis[4], Jan van Deursen[5], Floris Foijer[1], Alain de Bruin[2,3*], Ellen Nollen[1*]

[1] University of Groningen, University Medical Center Groningen, European Research Institute for the Biology of Aging, The Netherlands
[2] Department of Pediatrics, Division of Molecular Genetics, University Medical Center Groningen, The Netherlands
[3] Department of Pathology, Faculty of Veterinary Medicine, University of Utrecht, The Netherlands
[4] Department of Pediatrics, Molecular Genetics Section, University Medical Center Groningen, University of Groningen, the Netherlands.
[5] Department Pediatric and Adolescent Medicine and Department of Biochemistry and Molecular Biology, Mayo Clinic, United States of America

* The authors contributed equally

Abstract

Inactivation of the amyloid-promoting factors MOAG-4 and SERF suppresses the toxicity of neurodegenerative disease-related proteins in invertebrates and in human cell models for disease. However, the physiological consequences of their inactivation are unknown. To establish the potential of their therapeutic inhibition in disease, it is important to know the physiological consequences. Here, we generated *Serf2* knockout (*Serf2*$^{-/-}$) mice and investigate the role of Serf2 in the early stages of life. We show that deletion of *Serf2* results in neonatal death due to fetal atelectasis. In *Serf2*$^{-/-}$ pups, the lung tissue appeared not to be fully matured, and as a consequence these pups died of respiratory failure. Mouse embryonic fibroblasts (MEFs) from *Serf2*$^{-/-}$ embryos showed a delay in growth. Transcriptome analysis of these MEFs revealed significantly altered expression of cell cycle regulatory genes. Together, our study suggests that Serf2 either directly or indirectly regulates cell proliferation, which is important for embryonic growth and viability. The effect of *Serf2* deletion should be taken into account when exploring SERF2 inhibition as a therapeutic strategy to treat neurodegenerative disease.

Introduction

Aggregation-prone proteins are thought to cause age-related neurodegenerative diseases, like Alzheimer's and Huntington's disease, and suppression of their toxicity is explored as a therapeutic strategy to treat these diseases (Cohen et al., 2009; Kakkar et al., 2016; Thathiah et al., 2013). Genome-wide screens in model organisms have revealed several evolutionary conserved genetic pathways that regulate age-related protein toxicity (Bonini and Gitler, 2011; Gitler, 2007; Sin et al., 2014). Among these are the human orthologs of the *C. elegans* protein MOAG-4, the Small EDRK Rich Factors 1A and 2 (SERF1A and SERF2) that share 50% and 54% of their amino acid sequence identity to MOAG-4. Inactivation of MOAG-4 in *C. elegans* suppressed protein aggregation and toxicity of different aggregation-prone proteins and this function has been shown to be conserved for SERF1A and SERF2 in human cells expressing mutant huntingtin (van Ham et al., 2010). Even more, *in vitro* SERF1A has been shown to directly catalyze the amyloid formation of mutant huntingtin exon1, amyloid-beta, alpha-synuclein, and prion protein, suggesting that a direct interaction with the disease proteins drives their pathogenicity (Falsone et al., 2012). These findings make SERF an attractive target for inhibition of proteotoxicity in age-related diseases. However, the physiological consequences of SERF inactivation are unknown. Identifying its endogenous function is important, because it may reveal why SERF drives protein aggregation and toxicity at high age, and it will determines its potential as a target for inhibition. To establish its role in mammalian biology we generated *Serf2* knockout mice. We found that loss of *Serf2* results in neonatal lethality with incomplete penetrance, caused by fetal atelectasis at birth. *Serf2* knockout embryos and fibroblasts derived from these embryos show a delay in growth. Transcriptome analyses of these fibroblasts indicated gene expression changes that are enriched for cell-cycle regulatory genes. Together, our results show that loss of Serf2 delays cellular and embryonic growth, which results in incomplete lung development at birth and death because of respiratory failure.

Results

Knockout of *Serf2* in mice causes neonatal lethality with incomplete penetrance

To unravel the physiological function of the SERF, we aimed to generate full body knockout mice for *Serf1* and/or *Serf2*. We established to generate a *Serf2* knockout mouse (hereafter, *Serf2*$^{-/-}$). The *Serf2* gene is evolutionary highly conserved and consists of 3 exons located on chromosome 2 on the mouse genome, the protein contains 59 amino acid and the sequence is 100% identical between human and mice. Furthermore, *Serf2* is most similar to MOAG-4 and has only one human isoform. Disruption of the *Serf2* mouse gene was achieved by flanking exon 2 with *loxP* sites. Exon 2 was removed by *Cre*-mediated recombination of the *loxP* sites, by *Cre* expression under the *HPRT* promoter (Figure 1A). Mice lacking the *loxP*-flanked region of *Serf2* were identified by PCR genotyping analysis (Figure 1B). *Serf2* heterozygous and homozygous animal intercrosses resulted in only one *Serf2*$^{-/-}$ mouse at the age of 22 days, where 41 *Serf2*$^{-/-}$ mice were expected, according to Mendelian ratios ($p<0.001$, Figure 1E). To confirm loss of Serf2 we collected different organs of the *Serf2*$^{-/-}$ mouse and its littermates. Western blot and qPCR analyses confirmed complete loss of the Serf2 protein and RNA in the *Serf2*$^{-/-}$ mouse, and loss of about half of the Serf2 RNA expression in heterozygous mice in all the tested organs (Figure 1C and 1D). These results indicate that the *Serf2*$^{-/-}$ allele leads to loss of the Serf2 protein and RNA. Furthermore, loss of SERF2 leads to lethality with incomplete penetrance.

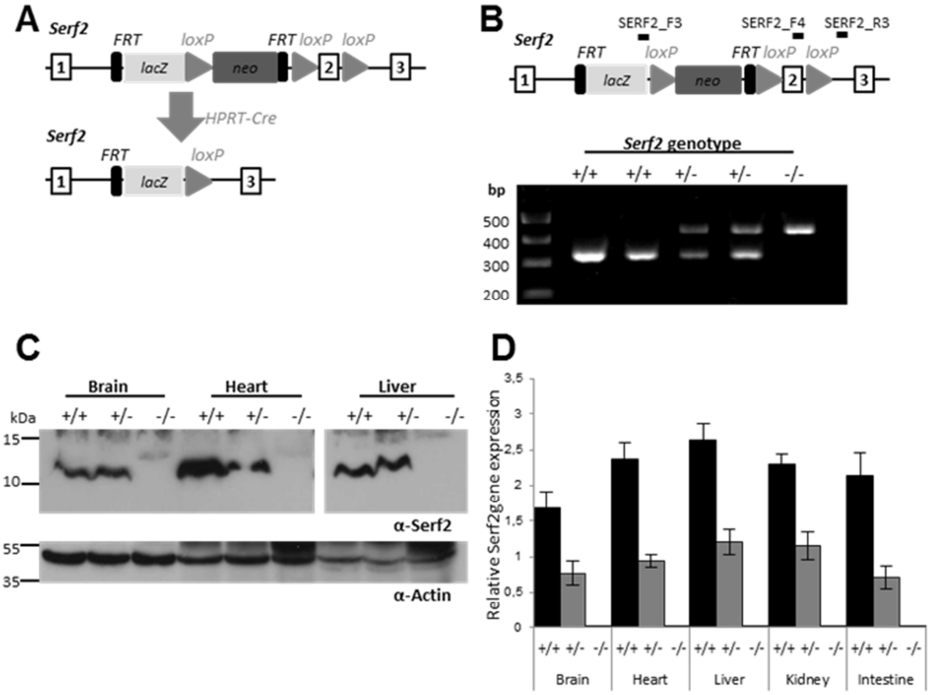

E

	Serf2$^{+/+}$	*Serf2*$^{+/-}$	*Serf2*$^{-/-}$	Unknown	Total
P22 (*Serf2*$^{-/-}$ x *Serf2*$^{+/-}$)		32	1***	1	34
Expected		17	17	9	
P22 (*Serf2*$^{+/-}$ x *Serf2*$^{+/-}$)	27	64	0***	5	96
Expected	24	48	24	0	

Figure 1. Serf2$^{-/-}$ mice are embryonically lethal with incomplete penetrance. (A) Targeting strategy used to delete exon 2 of Serf2 by using the 'knockout allele-First' (adjusted from Skarnes et al. 2011). Top panel: exon/intron structure of Serf2 including the positions of the LacZ and Neo cassettes, as well as loxP sites. Bottom panel: the Serf2 allele after recombination events as a result of crosses with HPRT-Cre mice. **(B)** Genotyping was performed using allele specific primers indicated by the black bars, SERF2_F3 and SERF2_R3 are used to amplify the knockout allele and SERF2_F2 and SERF2_R3 are used to amplify the wild type allele. **(C)** Western blot analysis of liver, heart and brain tissue of a Serf2$^{+/+}$, Serf2$^{+/-}$ and Serf2$^{-/-}$ adult mice to detect Serf2 and actin. **(D)** Real time RT-PCR analyses of Serf2 in different mouse tissues of adult mice, in the following genotypes Serf2$^{+/+}$ (n=3), Serf2$^{+/-}$ (n=8) and Serf2$^{-/-}$ (n=1), Serf2 levels were normalized to the housekeeping gene 18S (mean ± SEM). **(E)** Genotypic analyses of different crosses with original Serf2$^{+/-}$ and Serf2$^{-/-}$ mice *** ($p<0.001$; statistical test: Chi-square test).

Loss of Serf2 delays embryonic development

In order to investigate why loss of Serf2 causes reduced viability, we intercrossed *Serf2*$^{+/-}$ mice and analyzed the progeny at different stages of embryonic development. At E13.5, E15.5 and E17.5 *Serf2*$^{-/-}$ embryos were present in utero at the expected Mendelian ratios (Table 1). The *Serf2*$^{-/-}$ embryos had no Serf2 protein or RNA expression, and *Serf2*$^{+/-}$ embryos had approximately half of the Serf2 protein and RNA levels compared to their *Serf2*$^{+/+}$ littermates (Figure 2A and 2B). A significant reduction in overall size and weight was observed for the *Serf2*$^{-/-}$ embryos at E15.5 and E17.5, whereas no effect was observed in the *Serf2*$^{+/-}$ embryos (Figure 2C, 2D, 3A and 3B).

Table 1: Genotypes of *Serf2* embryos during different developmental stages

	***Serf2*$^{+/+}$**	***Serf2*$^{+/-}$**	***Serf2*$^{-/-}$**	**Total**
E13.5	8	15	7	30
Expected	*7,5*	*15*	*7,5*	
E15.5	10	30	11	51
Expected	*12,75*	*25,5*	*12,75*	
E17.5	7	19	8	34
Expected	8,5	17	8,5	
P0*	4	27	7 (5)[¥]	38
Expected	*9,5*	*19*	*9,5*	

[¥] 5 out of 7 animals died directly after birth, the other two animals showed trouble breathing but survived the first 30-60 minutes after birth

One possible explanation for the size and weight reduction could be the presence of placental abnormalities, which has been shown to result in embryonic growth delays, because of an impaired transfer of nutrient and oxygen to the embryo (Ward et al., 2012). We therefore analyzed the placentas of the Serf2$^{-/-}$ embryos at all embryonic stages and found no significant microscopic lesions in the placental labyrinth or other phenotypically differences at any of the three investigated time points, indicating that the reduction in embryo size is not due to placental defects but are rather due to loss of Serf2 in the embryo itself.

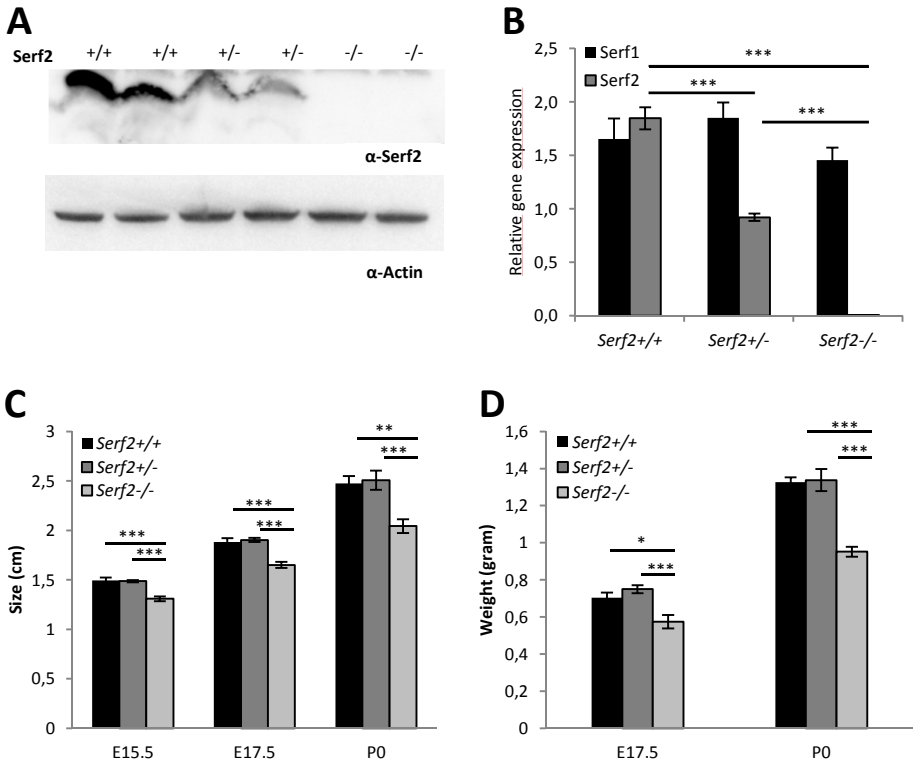

Figure 2. Loss of Serf2 delays embryonic development. (A) Western blot analyses of E13.5 *Serf2*$^{-/-}$, *Serf2*$^{+/-}$ and *Serf2*$^{+/+}$ embryos of Serf2 and actin. **(B)** Real time RT-PCR analyses of Serf1 and Serf2 in E13.5 heads, Serf gene expression was normalized to housekeeping gene beta-actin. (n=4, mean ± SEM, t-test ***p<0.001). **(C)** Length measurements in centimeters of the *Serf2*$^{-/-}$, *Serf2*$^{+/-}$ and *Serf2*$^{+/+}$ embryos at E15.5, E17.5 and P0 (mean ± SEM, t-test, **<0.01 ***, p<0.001). **(D)** Weight measurements in grams of the *Serf2*$^{-/-}$, *Serf2*$^{+/-}$ and *Serf2*$^{+/+}$ embryos and pups at E17.5 and P0 (mean ± SEM, t-test *<0.05, ***p<0.001).

To investigate embryonic phenotypes, we examined the embryos at different time points and found that at E17.5 the *Serf2*$^{-/-}$ embryos have a slight delay in development, particularly of the lung and kidney. The lung tissue of *Serf2*$^{-/-}$ embryos were slightly more condensed with less expanded alveoli compared to *Serf2*$^{+/+}$ embryos. The kidneys of *Serf2*$^{-/-}$ embryos show increased amount of mesenchyme with a lower number of tubules and differentiated glomeruli compared to *Serf2*$^{+/+}$ embryos (Figure 3C).

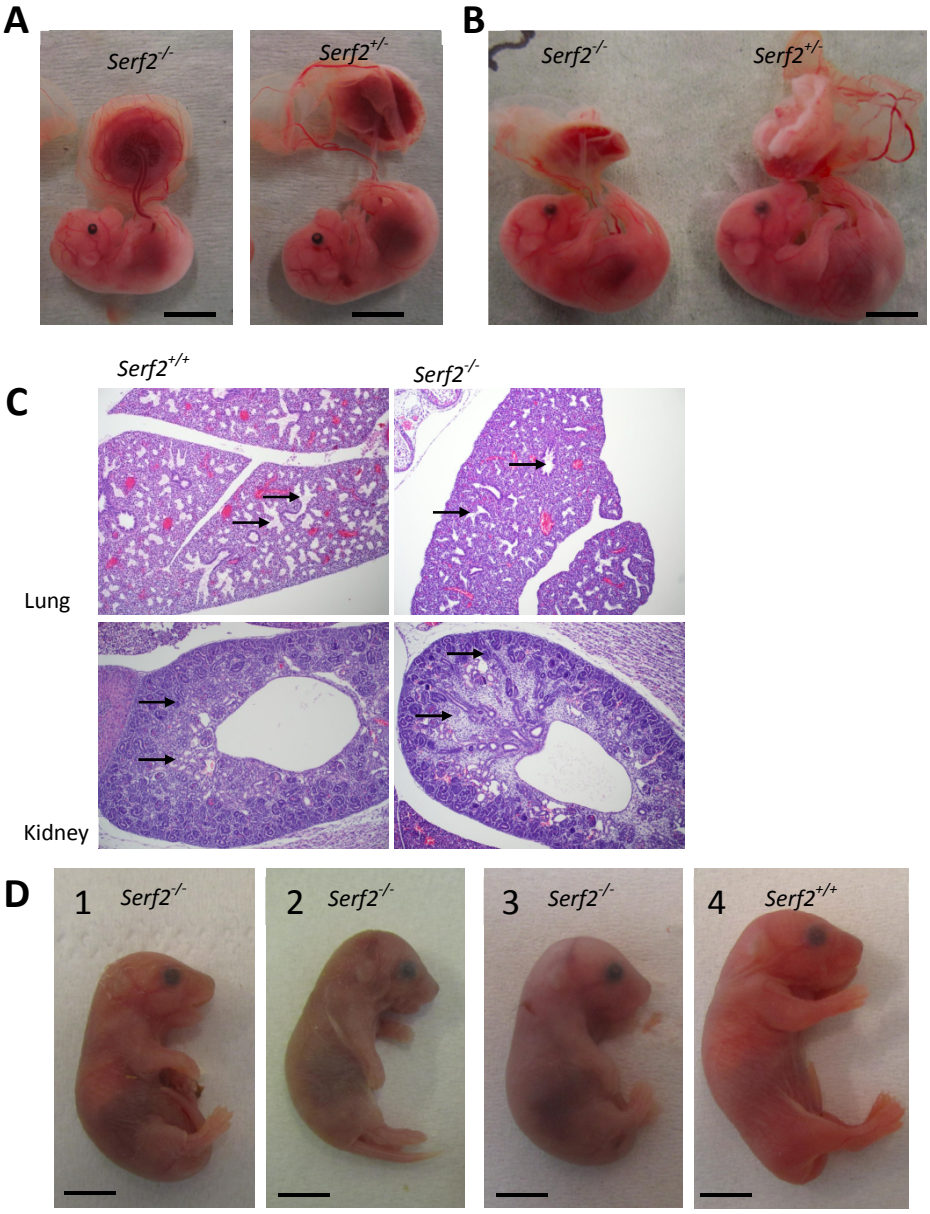

Figure 3. Loss of Serf2 delays embryonic development. (A) Lateral view of a *Serf2*$^{-/-}$ and *Serf2*$^{+/-}$ E15.5 embryo and placenta. **(B)** Lateral view of a *Serf2*$^{-/-}$ and *Serf2*$^{+/-}$ E17.5 embryo and placenta. **(C)** Hematoxylin and Eosin staining on *Serf2*$^{-/-}$ and *Serf2*$^{+/+}$ lung (arrows pointing at expanded bronchiole and alveoli) and kidney (arrows point at glomeruli and at mesenchyme) tissue at E17.5 (10 times magnification). **(D)** Lateral view of 3 *Serf2*$^{-/-}$ and 1 *Serf2*$^{+/+}$ P0 pup with three phenotypes, (1) pup born alive, (2) pup born dead, (3) pup born in the yolk sac and (4) healthy *Serf2*$^{+/+}$ pup (Scale bar 5 mm).

Altogether, the histologic appearance of the *Serf2*$^{-/-}$ tissues resembles gestational stage E16.5, indicating a delayed development of approximately 1 day. In comparison, *Serf2*$^{+/+}$ embryos from the same litter varied no more than half a day in the stage development, similar to what has previously been reported (Ward and Devor-Henneman, 2000). These observations indicate that the delayed embryonic development is caused by loss of Serf2 and not a result of natural variation between littermates.

Developmental delay of *Serf2*$^{-/-}$ mice results in fetal atelectasis and immature lung maturation

In order to establish the origin of neonatal death in these animals we observed them during delivery and in the following hour, the genotype determination of *Serf2* was done afterwards. *Serf2*$^{+/+}$ and *Serf2*$^{+/-}$ pups had a natural pink color, moved actively and were breathing regularly. For the *Serf2*$^{-/-}$ pups we observed three different phenotypes, (1) dead pups with white/greyish color that were born inside the intact yolk sac including the placenta, (2) grey pups that died directly after birth and (3) grey/pink colored living pups that moved less and showed troubled breathing (Figure 3D), suggesting the *Serf2*$^{-/-}$ pups were suffering from respiratory failure. All the *Serf2*$^{-/-}$ pups were born at a significantly smaller size and weight, with a reduced body weight of almost 30% (Figure 2C and 2D), as was expected from the observations at E15.5 and E17.5. Pathological analyses showed (partial) fetal atelectasis in all the *Serf2*$^{-/-}$ pups (Figure 4A). The ratio of saccular space was significantly lower in the *Serf2*$^{-/-}$ lungs compared to the *Serf2*$^{+/+}$ and *Serf2*$^{+/-}$ lungs (Figure 4B). This suggests that the lungs of the *Serf2*$^{-/-}$ pups were not yet fully maturated. In order to establish if the *Serf2*$^{-/-}$ lungs are indeed delayed in their maturation we examined cell proliferation in these tissues. We used a Ki67 antibody to establish the percentage of proliferative cells in lung, liver and kidney of P0 pups. This shows a trend towards an increase in the number of Ki67 positive cells in lung and liver tissue for the *Serf2*$^{-/-}$ pups, indicating that tissue differentiation was not yet completed (Figure 4C and 4D). To complement this finding, we measured the amount of cytoplasmic glycogen in the lungs, which indicates lung tissue maturity, because of its presence in immature epithelial lung cells. To detect the cytoplasmic glycogen we used periodic acid Schiff (PAS) staining in E17.5 embryos. An increase in PAS positive

staining was observed in the *Serf2*$^{-/-}$ embryos (Figure 4E and 4F). The higher number of cell proliferation and immature lung cells indicate that the lungs of *Serf2*$^{-/-}$ pups are not fully matured, and as a consequence these pups cannot breathe at birth and die of respiratory failure.

Furthermore, the dead *Serf2*$^{-/-}$ P0 pups showed minimal to moderate alteration in the muscle fibers of the diaphragm and intercostal muscle. These muscles are involved in expanding the lung volume, and include the thin fibers, muscle fiber degeneration and regeneration (Figure 4G). These results could indicate that the fetal atelectasis was caused by failure of these muscles to contract and thereby expanding the lung volume. This phenotype was not observed in the *Serf2*$^{-/-}$ pups that were alive after birth, they nevertheless show partial fetal atelectasis suggesting that the affected muscle fibers of the diaphragm and intercostal muscle are not the cause of the fetal atelectasis seen in the *Serf2*$^{-/-}$ pups, but could possibly worsen the phenotype.

Figure 4. The developmental delay *Serf2*$^{-/-}$ mice results in fetal atelectasis and immature lung maturation. (A) Hematoxylin and Eosin on *Serf2*$^{-/-}$ and *Serf2*$^{+/-}$ lung tissue, arrows point at saccular space. **(B)** Quantification of saccular space for *Serf2*$^{-/-}$ (n=7), *Serf2*$^{+/-}$ (n=6) and *Serf2*$^{+/+}$ (n=6) (mean ± SEM, t-test p<0.01). **(C)** Ki67 staining lung and liver tissue of *Serf2*$^{-/-}$ and *Serf2*$^{+/-}$ P0 pups (40x magnification). **(D)** Quantifications of the percentage of Ki67 positive cells in the lung, liver, and kidney for *Serf2*$^{-/-}$ (n=7), *Serf2*$^{+/-}$ (n=6) and *Serf2*$^{+/+}$ (n=6) (mean ± SEM, t-test, Lung p=0,1639, liver p=0,4369, kidney p=0,5848). **(E)** PAS staining on lung tissue of *Serf2*$^{-/-}$ and *Serf2*$^{+/+}$ E17.5 embryos scale bar 50 µm. **(F)** Quantifications of PAS staining/mm^2 in the lungs of *Serf2*$^{-/-}$ (n=7), *Serf2*$^{+/-}$ (n=6) and *Serf2*$^{+/+}$ (n=6) (mean ± SEM, t-test p=0.0842). **(G)** Hematoxylin and Eosin staining on *Serf2*$^{-/-}$ and *Serf2*$^{+/-}$ skeletal muscle at P0 at 10x magnification.

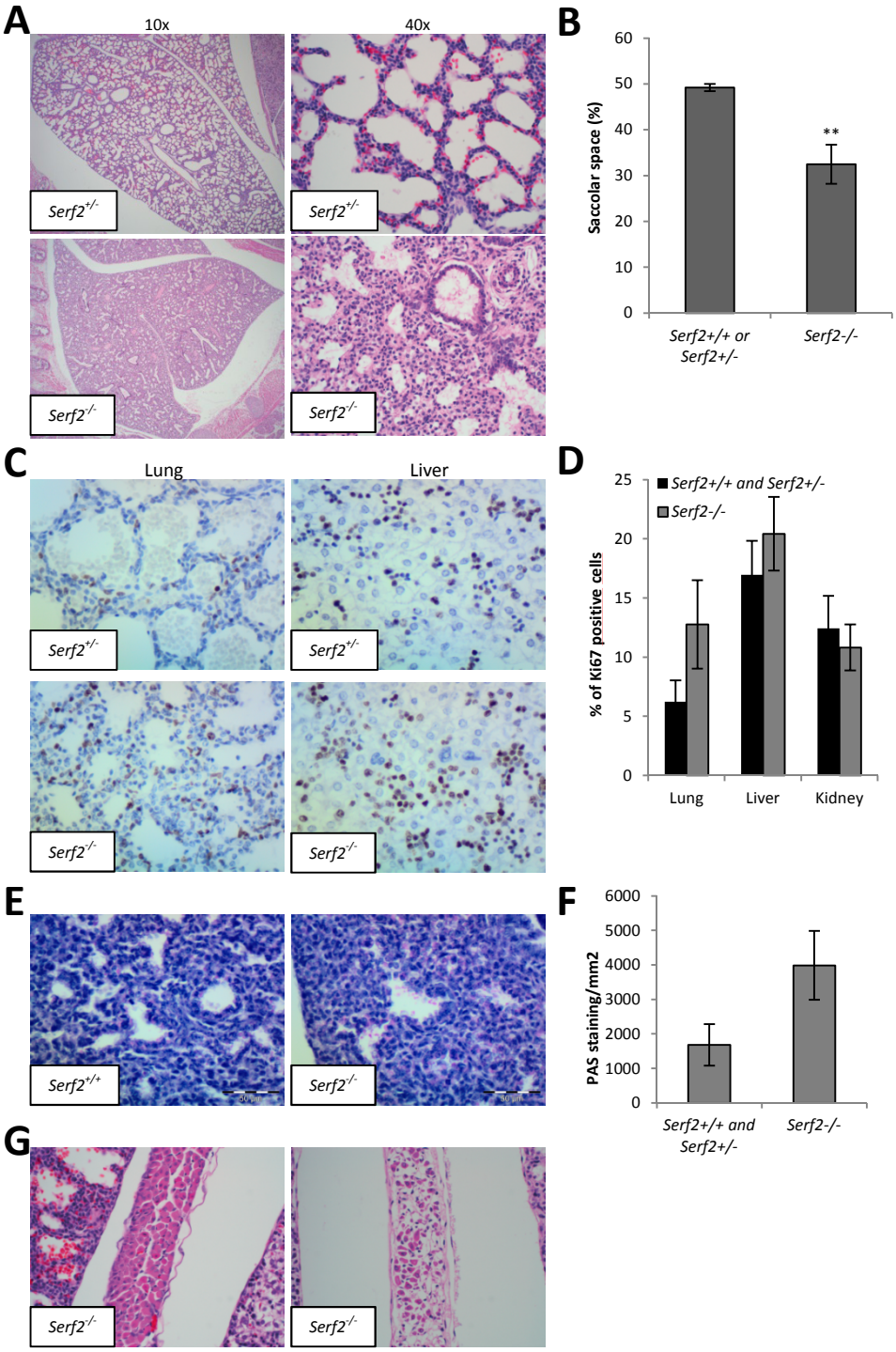
A
10x
40x
Serf2+/-
Serf2+/-
Serf2-/-
Serf2-/-
B
Saccolar space (%)
60
50
40
30
20
10
0
**
Serf2+/+ or Serf2+/-
Serf2-/-
C
Lung
Liver
Serf2+/-
Serf2+/-
Serf2-/-
Serf2-/-
D
Serf2+/+ and Serf2+/-
Serf2-/-
% of Ki67 positive cells
25
20
15
10
5
0
Lung
Liver
Kidney
E
Serf2+/+
Serf2-/-
F
PAS staining/mm2
6000
5000
4000
3000
2000
1000
0
Serf2+/+ and Serf2+/-
Serf2-/-
G
Serf2-/-
Serf2-/-

Loss of Serf2 alters regulation of cell cycle regulation genes

In order to explore the molecular mechanism behind the delayed development caused by *Serf2* depletion, we isolated mouse embryonic fibroblasts (MEFs) from E13.5 embryos. After two passages 3 independent *Serf2*$^{-/-}$ MEF cell lines and 4 independent *Serf2*$^{+/+}$ MEF cell lines were collected at approximately 70% confluency and processed for genome-wide transcriptomics. Analyses identified 738 genes that were significantly altered in the *Serf2*$^{-/-}$ MEFs ($p<0.05$) compared to *Serf2*$^{+/+}$ MEFs, among them, 348 genes were upregulated and 390 genes were downregulated. GO-term analysis linked a significant amount of genes to cell cycle related events (Table 2), including cell cycle, cell division and mitotic nuclear division. Most of the cell cycle related genes were upregulated in the *Serf2*$^{-/-}$ MEFs (Figure 5A). Next, we determined the connectivity between the enriched GO-terms. This analysis revealed three main clusters of biological functions of which genes are differentially regulated in the *Serf2*$^{-/-}$ MEFs; including cell cycle, but also cell adhesion and negative regulation of the apoptotic process (Figure 5B). KEGG pathway analyses also revealed an enrichment for cell cycle (Benjamini, $p<0.001$), focal adhesion (Benjamini, $p<0.001$), p53 signaling pathway (Benjamini, $p<0.01$) and regulation of actin cytoskeleton (Benjamini, $p<0.05$). Next we checked whether a growth difference would also be observed in the *Serf2*$^{-/-}$ MEFs and compared 3 *Serf2*$^{-/-}$ and 4 *Serf2*$^{+/+}$ MEF cell lines. Culturing these cells over several passages shows a clear trend of reduced cell growth in the *Serf2*$^{-/-}$ cell lines with a 37% reduction at P7 (Figure 5C, $p=0.31$, t-test). Together, these results show that loss of Serf2 has an impact on the cellular growth, and on the gene expression level at the cellular level.

Table 2: Go Term analysis, top 10 of biological functions of alternative expressed genes in the Serf2$^{-/-}$ MEFs by enrichment analysis using GO-term

GO ID	GO Term	% of List Total	Fold Enrichment	Benjamini	FDR
GO:0007049	cell cycle	7,57	2,46	0,0000	0,0000
GO:0030335	positive regulation of cell migration	3,71	3,65	0,0000	0,0000
GO:0051301	cell division	5,23	2,79	0,0000	0,0001
GO:0007067	mitotic nuclear division	4,26	3,07	0,0001	0,0002
GO:0016477	cell migration	3,30	3,45	0,0003	0,0009
GO:0001525	Angiogenesis	3,71	3,10	0,0003	0,0012
GO:0007229	integrin-mediated signaling pathway	2,06	4,43	0,0028	0,0117
GO:0050731	positive regulation of peptidyl-tyrosine phosphorylation	2,06	4,08	0,0064	0,0309
GO:0007160	cell-matrix adhesion	1,79	4,57	0,0078	0,0423
GO:0010628	positive regulation of gene expression	4,54	2,27	0,0079	0,0478

Discussion

Here we describe the investigation into the role of enhancer of protein aggregation Serf2 during early stages of life. The biological function of the Serf proteins other than their driving role in amyloid formation is still unknown. We found that loss of Serf2 in mice leads to neonatal death as a result of respiratory failure at birth, which is caused by immature lung development in combination with a fetal growth delay.

While deletion of the C.*elegans* homolog MOAG-4 has no effects on viability or life span (van Ham et al., 2010), the *Serf2*$^{-/-}$ mice died immediately or shortly after birth. Investigation into this reduced viability showed a reduction in size and weight as most prominent difference between *Serf2*$^{+/+}$/*Serf2*$^{+/-}$ and *Serf2*$^{-/-}$ embryos starting from E15.5 and onwards. As impaired transfer of nutrient and oxygen by the placenta can cause growth defects (Ward et al., 2012) we examined the *Serf2*$^{-/-}$ placentas and found no significant abnormalities in their labyrinth, suggesting that the growth delay is caused by loss of Serf2 in the embryos.

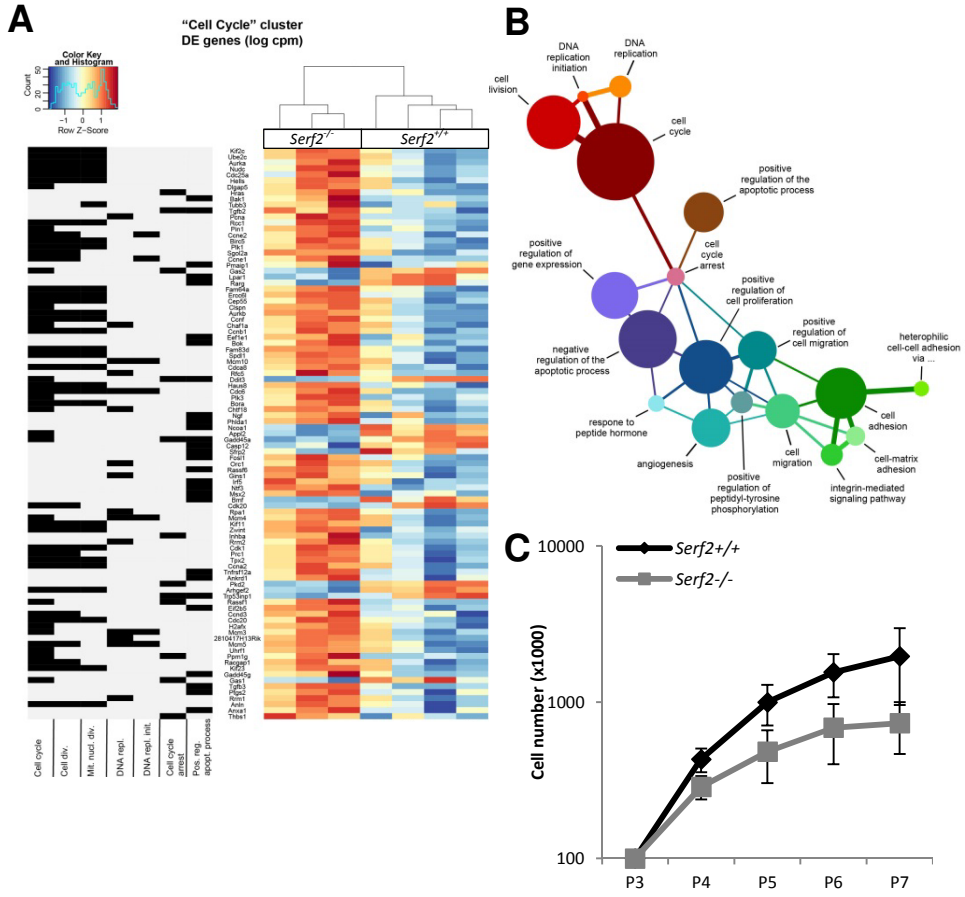

Figure 5. Loss of Serf2 results in altered gene expression enrichment of cell cycle related genes. **(A)** The hierarchical clustering of the up- and down-regulated genes in the *Serf2*$^{-/-}$ MEFs that are part of the cell cycle biological function according to GO-term analyses, the left clustering is sorted under the different cell cycle related clusters. **(B)** Diagram of GO-term clusters, circle size indicates amount of genes in the network, the bar thickness indicates amount of shared genes and bar color indicates the pathway that shares most genes. **(C)** 3T3 growth curve analyses with *Serf2*$^{+/+}$ (n=4) and *Serf2*$^{-/-}$ (n=3) MEFs (mean ± SEM, t-test, not significant)

Investigation into the *Serf2*$^{-/-}$ embryos resulted in a slight delayed development in the lungs and kidney of approximately 1 day in the E17.5 embryos. The small delay during embryogenesis resulted in a growth restriction of approximately 30% at birth. In addition to growth restriction at birth, the newborn *Serf2*$^{-/-}$ mice display (partial) fetal atelectasis. Fetal

atelectasis is known to have different origins. First it can be caused by insufficient production of surfactant, a lipoprotein complex formed by type II alveolar cells that lowers surface tension in the alveoli and thereby reduces the pressure gradient required to aerate the lungs during the first breath (Avery and Mead, 1959; Whitsett and Weaver, 2002). Secondly, fetal atelectasis can be the result of an undifferentiated state of the lung cells that is caused by delayed development (Whitsett et al., 2004). Lastly, fetal atelectasis can result from weakness in breath muscle activity, in which the diaphragm and intercostal muscles are not contracting enough to ensure increase of the lung volume (Fanaroff and Martin, 2002). In the dead *Serf2*$^{-/-}$ pups we observe that both the intercostal muscle and the diaphragm consists of thin muscle fibers that showed minimal to moderate muscle fiber degeneration and regeneration. This muscle phenotype might have made it difficult for the muscle to contract and thereby expanding the thoracic cavity, which therefore could lead to fetal atelectasis. However, in the *Serf2*$^{-/-}$ pups that did not die directly after birth, no changes in intercostal muscle or diaphragm was observed, still they had trouble breathing and showed partial fetal atelectasis. Indicating that fetal atelectasis in these animals is not caused by fiber thinning or muscle degeneration of the intercostal muscle or the diaphragm. However, the muscle degeneration could have worsened the atelectasis phenotype in the dead *Serf2*$^{-/-}$ pups.

In order to establish whether the lungs of the *Serf2*$^{-/-}$ pups were completely matured at birth we performed a KI67 antibody and PAS staining. This revealed a higher number of proliferating cells and immature cells in the lungs of *Serf2*$^{-/-}$ pups, indicating that these lungs were not fully matured yet, and as a consequence these pups were not able to breathe at birth and they died of respiratory failure. Neonatal breathing difficulty is one of the major causes of preterm infant mortality (Fanaroff and Martin, 2002). Many signaling molecules, receptors and transcription modulators have been identified to play a critical role in lung morphogenesis. Mutations have been linked to pathogenesis of severe lung disease at time of birth (Whitsett et al., 2004). Next to loss of *Serf2,* other knockout studies also observe fetal growth delay and fetal atelectasis. Other studies, in which gene deletion causes neonatal lethality as a result of fetal atelectasis and growth delay, are mostly involved in

general cellular pathways, such as ERK3 a member of the MAP kinase family (Klinger et al., 2009), STK40 a activator of ERK/MAPK signaling (Yu et al., 2013) and β arrestin 1 and 2 classical regulators of G-protein-coupled receptors (Zhang et al., 2010). Showing that disruption of genes involved in a general cellular pathway show a similar neonatal phenotype as loss of Serf2.

The overall small delay in development resulting in respiratory failure at birth does not resolve the unknown molecular function of Serf2. Therefore we examined the MEFs from these embryos for transcriptome analyses. We found that most alternatively expressed genes could be linked to cell cycle processes. Most of these cell cycle related genes were upregulated, while you would expect a down regulation when the growth delay is caused by lower cellular proliferation. One possible explanation is that the *Serf2*$^{-/-}$ MEFs are arrested in the cell cycle, caused by for example by DNA damage (Dasika et al., 1999). To investigate if the *Serf2*$^{-/-}$ MEFs are indeed arrested in their cell cycle it would be interesting to investigate the cell cycle profile and DNA damage in the *Serf2*$^{-/-}$ MEFs.

The effect of Serf2 on cell cycle gene regulation needs to be further established, because it could be troubling when using Serf2 inhibitors as long term therapeutic targets. *Serf2* inactivation might have a negative effect on growing cell populations in the human body. This could for example harm the stem cell pools of the body which could lead to unwanted side effects. However, no effect was observed on embryonic development in the heterozygous *Serf2* animals while having only half of the Serf2 expression, indicating that incomplete inactivation of *Serf2* might not have serious effects on growing cell populations, and might still have beneficial effects in neurodegenerative diseases. However, further research on the long term effect of *Serf2* depletion in the adult body is necessary to rule out any unwanted side effects.

Interestingly, most of the disease-causing aggregation-prone proteins are, like Serf2, highly conserved throughout evolution. While complete loss of some of these proteins results in early embryonic lethality, e.g. loss of huntingtin (Zeitling et al., 1995) and loss of TDP-43 (Kraemer et al., 2010) involved in respectively Huntington's disease and ALS, other disease-causing proteins have

one or more homologs that take over their function, only loss of all genes results in a phenotype, e.g. loss of both APP and APP pseudogene involved in Alzheimer's disease (Yang et al., 2005; Zheng et al., 1995) and loss of all three synucleins involved in Parkinson's disease (Greten-Harrison et al., 2010). Together showing the importance of these proteins during development and early life. Because the disease manifestations in neurodegenerative diseases are caused long after reproduction, disease severity appears to be determined in part by genetic variation. Given that Serf has been discovered as a modifier of amyloid formation, but appears to have an important role early in life, it might be possible that is has a role in the early life which is linked with these aggregation-prone proteins. Alternatively, the role of Serf in development is unrelated to its interactions with disease proteins and only with old age does this interaction become problematic.

In summary, we show that Serf2 is essential for embryonic and cellular growth. The embryonic growth delay results in death of *Serf2*$^{-/-}$ pups at birth due to incomplete lung maturation. However, more research into the molecular function of *Serf2* is necessary to unravel how *Serf2* affects cell cycle and how this relates to its normal function.

Experimental procedures

Animals

All experiments were approved by the Institutional Animal Care and Use Committee of the University of Groningen (Groningen, The Netherlands). All mice were maintained on a C57BL/6J background and housed in a 12:12 hour light/dark cycle and the animals had ad libitum access to food and water.

For genotyping, DNA from tail and yolk sac biopsies was purified using prepGEM® Tissue kit according to a protocol adapted from the manufacturer (ZYGEPTI0500, ZyGEM, VWR International BV) and subjected to PCR. The wild type allele was amplified using the following two primers, SERF2_*F4: GATGATGGGCTTTCTGCTGC* and *SERF2_R3:* CTTGATATGTGAAGCCCCTGC resulting in a 335 base pair product. The knockout allele was amplified using the following primers, *SERF2_F3:* CCGGTCGCTACCATTACCAG and *SERF2_R3:* CTTGATATGTGAAGCCCCTGC resulting in a 420 base pair product. Products were visualized on a 2% agarose gel.

Embryo processing and immunohistochemistry

Embryos were fixed in 4% formalin (Kinipath) for a minimum of 24 hours at room temperature. For the pathological analysis the embryos and their placenta were cut bisected longitudinally and embedded in paraffin, they were cut using the microm HM 340E (Thermo Scientific).

For the hematoxylin and eosin staining 4 µm sections were incubated at 60°C for 15 minutes followed by deparaffinization and rehydration in xylene (2x), 100% alcohol (2x), 96% alcohol, 70% alcohol and water. Next, 4 minute incubation with hematoxylin, 10 minutes water, 1 minute eosin and 10 seconds water, followed by dehydration in 70% alcohol, 96% alcohol, 100% alcohol (2x) and xylene (2x).

For the PAS staining 3 µm sections were dried overnight at 60°C and deparaffinized and rehydrated in xylene (2x), 100% alcohol (2x), 96% alcohol, 70% alcohol and water. Next the sections were incubated in 1% periodic acid for 2 minutes and rinsed with water, incubated for 8 minutes in the dark in Schiff's reagent, rinsed and counterstained with hematoxylin and dehydration in 70% alcohol, 96% alcohol, 100% alcohol (2x) and xylene (2x).

For the Ki67 immunostaining, 4 µm sections were dried overnight at 55°C and deparaffinized and rehydrated in xylene (2x), 100% alcohol (2x), 96% alcohol, 70%

alcohol and water. Followed by antigen retrieval in citrate buffer (pH 6.0) and blocking endogenous peroxidase activity in 1% H_2O_2 in methanol for 30 minutes. Next, incubation with 10% goat serum for 30 minutes and overnight incubation with primary Ki67 antibody (1/250, Fisher scientific, RM-9106-s0). The next day the section was incubated with the anti-goat biotinylated secondary antibody (1/500, Vector, BA-1000) for 2 hours. Next, sections were incubated in ABC complex (Vector, PK-4000) for 30 minutes and reacted with diamino-benzidine (0.5 mg/ml H_2O with 0.01% H_2O_2) for 10 minutes, counterstained with hematoxylin and dehydration in 70% alcohol (2x), 96% alcohol (2x), 100% alcohol (2x) and xylene (2x).

Quantitative RT-PCR

Total RNA was extracted using TRIzol Reagent (Life Technologies) according to the manufacturers' description. Total RNA quality and concentration were assessed using a NanoDrop 2000 spectrophotometer (Thermo Scientific/Isogen Life Science). cDNA was made from 1,5 µg total RNA with a RevertAid H Minus First Strand cDNA Synthesis kit (Thermo Scientific) using random hexamer primers.

Quantitative real-time PCR was performed using a Roche LightCycler 480 Instrument II (Roche Diagnostics) with SYBR green dye (Bio-Rad Laboratories) to detect DNA amplification. Relative transcript levels were quantitated using a standard curve of pooled cDNA solutions. Expression levels were normalized to 18S mRNA levels. The primers for Quantitative PCR are 18S-F: CGGACAGGATTGACAGATTG, 18S-R: CAAATCGCTCCACCAACTAA, Serf2-F: CCGCGGTAACCAGCGAGAGC, Serf2-R: TCCGAGTCCCTCTGCTTGCG, SERF1-F: TGGCCCGTGGAATCAAAGAGAAA, SERF1-R: TGCATGATCTCTGAATCCCTCTGCT.

Western Blot analysis

Tissues were homogenized in RIPA buffer (50 mM Tris pH 8, 150 mM NaCl, 5mM EDTA, 0.5% SDS, 0.5% SDO, 1% NP-40) with protease inhibitor cocktail (Roche) and incubated on ice for one hour, spun down at 13.300 rpm for 30 min at 4°C and the supernatant was collected. For protein measurement a BCA kit was used, for Serf2 analyses 150 µg was loaded on a 10-20% tris/tricine SDS-page gels (Bio-Rad Laboratories) and blotted onto 0,2 µm nitrocellulose membrane (Bio-Rad Laboratories). Membranes were incubated O/N with Serf2 (1/1500, Protein tech) or Actin (1/10.000, MP biomedicals) antibody. Next, the membranes were incubated with anti-mouse or –rabbit secondary antibodies tagged with horseradish peroxidase (1/10.000, Bio-Rad Laboratories) for one hour at room temperature and visualized by chemiluminescence (Amersham ECL prime western blotting detection reagent, VWR).

Cell culture and growth assays

Serf2$^{+/+}$, *Serf2*$^{+/-}$ and *Serf2*$^{-/-}$ MEFs were isolated from E13.5 embryos. MEFs were cultured in T75 culture flasks (Greiner Bio-One, 658175), high–glucose Dulbecco's modified Eagle's medium (Gibco), supplemented with 10% fetal bovine serum (Sigma 12133C), 1% penicillin/streptomycin (Gibco), non-essential amino acids (Gibco) and β-mercaptoethanol at 37°C, 5% CO_2 and 3% O_2. The 3T3 assay was done in triplicate, 100.000 cells were plated in 6 wells plates (Greiner Bio-One, 657160) and counted every third day, of which 100.000 cells were plated on new 6 wells plate (Greiner Bio-One, 657160) and so on.

RNA sequencing

RNA sequencing analysis was performed on 3 MEF cell lines from *Serf2*$^{-/-}$ mice and 4 *Serf2*$^{+/+}$ littermate controls. Total RNA was isolated from MEFs using the Qiagen RNeasy isolation kit. Integrity of the RNA based on RIN scores as determined by a Bioanalyzer (Agilent). RNA-sequencing libraries were prepared using TruSeq Stranded Total RNA with Ribo-Zero Human/Mouse/Rat (RS-122-2201; Illumina, CA, USA) according to manufacturers' protocol. Pooled libraries were sequenced on an Illumina HiSeq 2500 (single-end 50 bp). Reads were aligned to the mouse reference genome (mm10) using a splicing-aware aligner (StarAligner). Aligned reads were FPM normalized, excluding low abundance genes (mean FPM>1 in at least two samples). The raw count data were preprocessed with the use of the programming language R (3.4.0) [R Core Team, 2016, available online at: www.r-project.org], the program RStudio (1.0.143) [RStudio Team, 2016, available online at: http://www.rstudio.com/] and the EdgeR package (3.18.0)(Robinson et al., 2010). Genes that displayed a fragment per million (FPM) value > 1 in at least two libraries were retained, resulting in a list of 12808 genes for differential analysis. Differentially expressed (DE) genes between the *Serf2*$^{+/+}$ and *Serf2*$^{-/-}$ MEFs were identified using the EdgeR general linear model approach. After statistical correction for multiple comparisons with the "false discovery rate" (FDR) method (FDR<0.05), a list of 738 DE genes was obtained. DAVID (6.8) was used to perform functional annotation analyses on this gene list and to identify significantly enriched gene ontology (GO) terms [using GOTERM_BP_DIRECT] and KEGG pathways (Huang et al., 2009a, 2009b). The connectivity between the enriched GO terms was further examined by determining the amount of DE genes shared between the different GO terms. We defined parent-child relationships between the GO terms based on the percentage of the total amount of DE genes in that GO term that was shared. The GO term that shared the highest percentage of its DE genes was considered the child of the other GO term in that relationship. The most

significant relationships (where the child shared > 25% of its genes) were mapped using the igraph package (1.0.1). Three GO terms were found to have multiple children and no parent. We defined three clusters of GO terms surrounding these parent GO tems. Children were always clustered with the parent with whom they shared the strongest connection. One GO term, positive regulation of the apoptotic process, showed no child relation with one of the clusters and was therefore connected to the only cluster it had a significant connection with. Heat maps were generated containing the full list of DE genes for each GO term cluster.

Author contributions

E.S., F.F., A.B. and E.A.A.N. designed the experiments. E.S., L.J., O.S., W.H., B.B., M.K., L.H. and S.Y. performed experiments and analyses. B.S. and J.D. provided the Serf2 mice. E.S. and E.A.A.N. wrote the manuscript.

Acknowledgements

We thank Freek Sorgdrager for technical assistance with the P0 experiments, and Petra Bakker for technical assistance with RNA library preparations. This work was supported by the European Research Council (ERC) starting grant (to E.A.A.N.) and the Alumni chapter Gooische Groningers facilitated by the Ubbo Emmius Fund.

References

Avery, M. E., and Mead, J. (1959). Surface properties in relation to atelectasis and hyaline membrane disease. *AMA J. Dis. Child* 97, 517–523.

Bonini, N. M., and Gitler, A. D. (2011). Model organisms reveal insight into human neurodegenerative disease: Ataxin-2 intermediate-length polyglutamine expansions are a risk factor for ALS. *J. Mol. Neurosci.* 45, 676–683. doi:10.1007/s12031-011-9548-9.

Cohen, E., Paulsson, J. F., Blinder, P., Burstyn-Cohen, T., Du, D., Estepa, G., et al. (2009). Reduced IGF-1 signaling delays age-associated proteotoxicity in mice. *Cell* 139, 1157–1169. doi:10.1016/j.cell.2009.11.014.

Dasika, G. K., Lin, S. C., Zhao, S., Sung, P., Tomkinson, A., and Lee, E. Y. (1999). DNA damage-induced cell cycle checkpoints and DNA strand break repair in development and tumorigenesis. *Oncogene* 18, 7883–99. doi:10.1038/sj.onc.1203283.

Falsone, S. F., Meyer, N. H., Schrank, E., Leitinger, G., Pham, C. L. L., Fodero-Tavoletti, M. T., et al. (2012). SERF protein is a direct modifier of amyloid fiber assembly. *Cell Rep.* 2, 358–371. doi:doi: 10.1016/j.celrep.2012.06.012.

Fanaroff, A., and Martin, R. (2002). “Fanaroff and Martin`s Neonatal-perinatal medicine: Diseases of the Fetus and Infant,” in, 1001–1011.

Gitler, A. D. (2007). Beer and bread to brains and beyond: Can yeast cells teach us about neurodegenerative disease? *NeuroSignals* 16, 52–62. doi:10.1159/000109759.

Greten-Harrison, B., Polydoro, M., Morimoto-Tomita, M., Diao, L., Williams, A., Nie, E., et al. (2010). αβγ -Synuclein triple knockout mice reveal age-dependent neuronal dysfunction. *Proc. Natl. Acad. Sci.* 107, 19573–19578. doi:10.1073/pnas.1005005107.

Huang, D., Sherman, B., and Lempicki, R. (2009a). Bioinformatics enrichment tools: paths toward the comprehensive functional analysis of large gene lists. *Nucleic Acids Res.* 37, 1–13. doi:10.1093/nar/gkn923.

Huang, D., Sherman, B., and Lempicki, R. (2009b). Systematic and integrative analysis of large gene lists using DAVID Bioinformatics Resources. *Nat. Protoc.* 4, 44–57.

Kakkar, V., Mansson, C., and de Mattos, E. P. (2016). The S/T-Rich Motif in the DNAJB6 Chaperone Delays Polyglutamine Aggregation and the Onset of Disease in a Mouse Model. *Mol. Cell* 62, 272–283. doi:10.1016/j.molcel.2016.03.017.

Klinger, S., Turgeon, B., Lé Vesque, K., Wood, G. A., Aagaard-Tillery, K. M., and Meloche, S. (2009). Loss of Erk3 function in mice leads to intrauterine growth restriction, pulmonary immaturity, and neonatal lethality. *Proc. Natl. Acad. Sci.* 106, 16710–16715. doi:10.1073?pnas.0900919106.

Kraemer, B. C., Schuck, T., Wheeler, J. M.,

Robinson, L. C., Trojanowski, J. Q., Lee, V. M. Y., et al. (2010). Loss of Murine TDP-43 disrupts motor function and plays an essential role in embryogenesis. *Acta Neuropathol.* 119, 409–419. doi:10.1007/s00401-010-0659-0.

Robinson, M., McCarthy, D., and Smyth, G. (2010). Bioconductor package for differential expression analysis of digital gene expression data. *Bioinformatics* 26, 139–140. doi:10.1093/bioinformatics/.

Sin, O., Michels, H., and Nollen, E. A. A. (2014). Genetic screens in Caenorhabditis elegans models for neurodegenerative diseases. *Biochim. Biophys. Acta - Mol. Basis Dis.* 1842, 1951–1959. doi:10.1016/j.bbadis.2014.01.015.

Thathiah, A., Horré, K., Snellinx, A., Vandewyer, E., Huang, Y., Ciesielska, M., et al. (2013). β-arrestin 2 regulates Aβ generation and γ-secretase activity in Alzheimer's disease. *Nat. Med.* 19, 43–49. doi:10.1038/nm.3023.

van Ham, T. J., Holmberg, M. A., van der Goot, A. T., Teuling, E., Garcia-Arencibia, M., Kim, H. eui, et al. (2010). Identification of MOAG-4/SERF as a regulator of age-related proteotoxicity. *Cell* 142, 601–612. doi:10.1016/j.cell.2010.07.020.

Ward, J. M., and Devor-Henneman, D. E. (2000). Gestational mortality in genetically engineered mice: evaluating the extraembryonal embryonic placenta and membranes. *Pathol. Genet. Eng. mice*, 103–122.

Ward, J. M., Elmore, S. A., and Foley, J. F. (2012). Pathology Methods for the Evaluation of Embryonic and Perinatal Developmental Defects and Lethality in Genetically Engineered Mice. *Vet. Pathol.* 49, 71–84. doi:10.1177/0300985811429811.

Whitsett, J. A., and Weaver, T. (2002). Hydrophobic surfactant proteins in lung funtion and disease. *N. Engl. J. Med.* 347, 2141–2148. doi:10.1056/NEJMra022387.

Whitsett, J. A., Wert, S. E., and Trapnell, B. C. (2004). Genetic disorders influencing lung formation and function at birth. *Hum. Mol. Genet.* 13, 207–215. doi:10.1093/hmg/ddh252.

Yang, G., Gong, Y. D., Gong, K., Jiang, W. L., Kwon, E., and Al, E. (2005). Reduced synaptic vesicle density and active zone size in mice lacking amyloid precursor protein (APP) and APP-like protein 2. *Neurosci. Lett.* 384, 66–71. doi:10.1016/j.neulet.2005.04.040.

Yu, H., He, K., Li, L., Sun, L., Tang, F., Li, R., et al. (2013). Deletion of STK40 protein in mice causes respiratory failure and death at birth. *J. Biol. Chem.* 288, 5342–5352. doi:10.1074/jbc.M112.409433.

Zeitling, S., Liu, J.-P., Chapman, D., Papaioannou, V., and Efstratiadis, A. (1995). Increased apoptosis and early emryonic lethality in mice nullizygous for the Huntington's disease gene homologue. *Nature* 11, 155–163. doi:10.1038/ng1095-155.

Zhang, M., Liu, X., Zhang, Y., and Zhao, J. (2010). Loss of βarrestin1 and βarrestin2 contributes to pulmonary hypoplasia and neonatal lethality in mice. *Dev. Biol.* 339, 407–417. doi:10.1016/j.ydbio.2009.12.042.

Zheng, H., Jiang, M., Trumbauer, M. E., Sirinathsinghji, D. J. S., and Al, E. (1995). β-Amyloid precursor protein-deficient mice show reactive gliosis and decreased locomotor activity. *Cell* 81, 525–531.